

A Dynamic Similarity Index for Assessing Voltage Source Behaviour in Power Systems

Onur Alican, *Student Member, IEEE*, Dionysios Moutvelis, *Member, IEEE*, Josep Arévalo-Soler, *Student Member, IEEE*, Carlos Collados-Rodriguez, *Member, IEEE*, Jaume Amorós, Oriol Gomis-Bellmunt, *Fellow, IEEE*, Marc Cheah-Mañe, *Member, IEEE*, Eduardo Prieto-Araujo, *Senior Member, IEEE*

Abstract—Due to the fundamental transition to a power electronic dominated power system, the increasing diversity of dynamic elements underscores the need to assess their similarity to mature electrical engineering models. This article addresses the concept of the Dynamic Similarity Index (DSI) for its use in, power electronics-dominated networks. The DSI is a multi-purpose tool developed to be used by different stakeholders (e.g., converter manufacturers and system operators). Such an index is calculated per frequency, which serves to anticipate potential differences in particular frequency ranges of interest between the model under study and the reference model. Within the scope of this study, the dynamic similarity of inverter-based generators to an ideal voltage source behind an impedance is assessed, due to the relevance of this fundamental circuit in the representation of generation units in power system studies. The article presents two potential applications based on this mathematical framework. First, for manufacturers to evaluate control performance compared to a reference model and second, it enables operators to diagnose buses with voltage vulnerability based on a user-defined reference Short-Circuit Ratio (SCR) value. The DSI results for these two case studies are validated using Matlab Simulink simulations.

Index Terms—dynamic similarity index, voltage source behavior, inverter-based resource, voltage stiffness

I. INTRODUCTION

A. Motivation

Traditional power systems exhibit high Voltage Source Behaviour (VSB) due to the Synchronous Generator (SG) capability to impose system voltage and phase angle [1]. Also, since the impedances of SG stators are not negligible, SGs are typically represented as voltage sources behind an impedance in power system stability and converter integration studies [2]. However, due to the increasing need for decarbonization, SGs are gradually replaced by Inverter-Based Resources (IBRs). Conventional controllers of such IBRs often exhibit limited VSB, compared to SGs, which leads to increased grid voltage variations against disturbances [3,4]. The ideal VSB of a device consists in maintaining constant both the magnitude and the phase angle of the voltage at its connection point under any disturbance. This requires the capability to instantaneously inject or absorb any amount of current during the disturbance, something unfeasible in practice [5]. For this reason in practical scenarios, Transmission System Operators (TSOs) may require a Voltage Source behind an Impedance (VSbI) characteristic in a frequency range of 5 Hz to 1 kHz to avoid detrimental controller interactions as well as to maintain voltage stability [6,7]. In this context, the capability to quantify

the dynamic similarity of various generators, both conventional and inverter-based, to an ideal VSbI characteristics is highly desirable for both component control design and system-wide analysis.

B. Literature Review

The resemblance of IBRs to a VSbI with regards to their dynamic operation highly depends on their control structure. The IBR controllers are typically categorized between Grid-Following (GFL) and Grid-Forming (GFM), based on their capability, or lack thereof, to regulate the voltage and frequency at their connection point. GFL converters use a Phased-Locked Loop (PLL) that tracks the voltage of the grid and estimates its angle, which is then used in the converter control. This leads to potential instabilities of GFL converters under weak grid conditions [8]. Moreover, since PLL tracks the grid voltage and estimate angle, GFL converters are intended to inject current into the grid within its limits [9]. For the above reasons, GFL converters are usually represented by current sources in sub-transient time frames [10,11]. However, this representation is not unique, since GFL converters can be assembled with various control strategies that have different tuning options. Therefore, quantifying the dynamic similarity between VSbI and GFL-IBRs is of interest.

GFM converters are capable of imposing the voltage and angle at their connection bus by means of a dedicated voltage controller. For this reason, they are usually represented as VSbI from the grid perspective in the sub-transient to the transient time frame [11]. Due to the different available control topologies (e.g., droop control, Virtual Synchronous Machine (VSM) and Virtual Oscillator Control (VOC) [12]) and the wide range for the controller parameter selection, quantifying the level of VSbI behaviour of each GFM-IBR exhibits is not straightforward.

The VSB of generation units is also indicative of potential interactions between them. Generation units with high VSB, which are located electrically close or connected to a strong grid, may induce oscillations and interact between them or with the network, leading to instability [13,14]. For this reason, the ability to quantify the VSbI of each generation unit, depending on their control mode and control parameter selection, would be beneficial for its control design and for system-level planning.

In the literature, there have been limited studies that systematically quantify the VSB of different generation units. In [15],

the authors propose a voltage stiffness index that considers the impedance and phase angle between the network and the different interconnected devices at the fundamental frequency. However, it would be beneficial to assess the VSB of generators across a wide frequency range. In references [16, 17], the authors describe a frequency-scan-based characterization of GFM and GFL modes. However, an analytical link between the oscillation modes and the VSB of the generation units is not included. Later in [18], the authors compare the VSB of various GFM inner control techniques with a VSBI in both time and frequency domains. In this study, GFL converters are not considered. Finally, in [19] the voltage source behavior of GFM and GFL are mathematically compared by using singular values. Also, the effect of different control topologies on the voltage source behavior of GFM is shown. However, various tuning options of GFL and its effect on the VSB is not studied.

The similarity between different dynamical systems can be observed in several ways. Modal analysis fully captures the damping ratio and frequency of all the system modes [20]. However, when the order of the system is large, inspecting all the system modes is not straightforward. Applying a perturbation and comparing the time-domain signals of different systems is an alternative way to assess the dynamic similarity between them. The shortcoming of this approach is that the different dynamics of the system are unequally excited from each disturbance, limiting the accuracy of the observed results for the full frequency spectrum of interest. Finally, assessing the dynamic similarity in the frequency domain provides information across the full dynamical spectrum. However, the typical representation of power system devices using rotating reference frames in the frequency domain consists of defining a 2×2 Multiple-Input Multiple-Output (MIMO) system, leading to four frequency domain plots to observe the full dynamic operation of the studied systems [21]. The proposed Dynamic Similarity Index (DSI) method overcomes all these issues by quantifying the maximum amplification of the error in a single plot at all frequencies, within a rotating reference frame modelling approach.

C. Contribution

In this paper, the DSI concept is introduced for different applications. By selecting VSBI as a reference, note any reference can be selected depending on the study) first, the VSB of both GFL and GFM converter with different control configurations is shown. Then, the index is applied on the system level to identify which parts of the network has different value with respect to the reference. The contributions of this paper can be summarized as follows:

- A novel metric, (DSI), is presented to evaluate the dynamic similarity between two systems, is proposed. The DSI is calculated in the frequency domain in MIMO systems.
- The proposed index is applied to show the effect that various operational modes and control parameter selections of IBRs have on their VSB assessment. Such an application can be useful for converter manufacturers or consultancy companies to reveal the impact of the converter control setup on the network operation.

- Finally, the DSI is used for the identification of buses that have high/low VSB in a 100% IBR based network. This information can help TSOs determine critical connection points for newly-commissioned IBRs and their suitable control structures.

Note that, such applications are just example usages of the methodology. Other operations of the methodology might arise. The results are supported by simulations for two case studies based on well-known benchmarks, including the IEEE 9-bus to illustrate the concept and 118-bus systems showcase it in a larger network.

D. Paper Organization

The organization of the rest of the paper is the following. The VSBI behavior is derived analytically and studied in the frequency domain in Section II. In Section III, the DSI and its applications are introduced. Section IV presents the case studies while Section V concludes the paper and suggests future research directions.

II. DSI REFERENCE MODEL SELECTION

This section aims to provide insights for the reference selection, since this is critical for assessing the dynamic similarity of a system. Note that, in this work, the reference selection is based on a model of a VSBI. To this end, the small-signal dynamic characteristics of a VSBI are first analytically derived by using impedance analysis. Then, an example system, consisting of two voltage sources, one representing the system under study and the other external grid, is used to illustrate the effect of the VSBI parameters on the overall system dynamic performance. The specification and analytic derivation of the desired dynamic characteristics of a voltage source will then be leveraged in Sections III and IV to be used as a reference for the DSI calculation.

A. Impedance Analysis Preliminaries

The starting point is the representation of a power system as a set of nonlinear ordinary differential equations in the form of [1]

$$\frac{d\mathbf{x}}{dt} = \mathbf{f}(\mathbf{x}, \mathbf{u}) \quad (1)$$

where $\mathbf{x} = \mathbf{x}(t) : \mathbb{R}^n$ and $\mathbf{u} = \mathbf{u}(t) : \mathbb{R}^m$ are column vectors of state and input variables, respectively, $\mathbf{f} : \mathbb{R}^{n+m} \rightarrow \mathbb{R}^n$ is a nonlinear function and n, m are the number of states and inputs, respectively. One should note that the representation of (1) is general and can always be achieved [22, 23]. By linearizing (1) and selecting k number of outputs, the linear state-space model of the system is represented as follows [24]

$$\begin{aligned} \frac{d\Delta\mathbf{x}}{dt} &= \mathbf{A}\Delta\mathbf{x} + \mathbf{B}\Delta\mathbf{u} \\ \Delta\mathbf{y} &= \mathbf{C}\Delta\mathbf{x} + \mathbf{D}\Delta\mathbf{u} \end{aligned} \quad (2)$$

where $\mathbf{y} = \mathbf{y}(t) : \mathbb{R}^k$ is the output column vector, $\mathbf{A} \in \mathbb{R}^{n \times n}$, $\mathbf{B} \in \mathbb{R}^{n \times m}$, $\mathbf{C} \in \mathbb{R}^{k \times n}$, and $\mathbf{D} \in \mathbb{R}^{k \times m}$ are the state, input, output and feedforward matrices, respectively. From the state-space representation, the Transfer Functions (TFs) between the

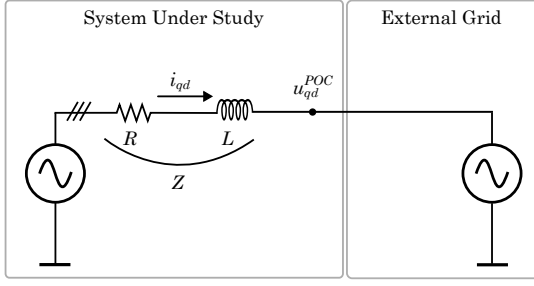


Fig. 1. Single-line diagram of a simple radial system with 2 voltage sources behind an impedance. Z (System Under Study) and (External Grid)

system inputs and outputs in the Laplace domain are derived using

$$\frac{\mathbf{y}(s)}{\mathbf{u}(s)} = \mathbf{C}(s\mathbf{I} - \mathbf{A})^{-1}\mathbf{B} + \mathbf{D} \quad (3)$$

where s is the Laplace operator, and $\mathbf{u}(s)$, $\mathbf{y}(s)$ are the input and output functions, respectively, in the Laplace domain. When these inputs/outputs refer to the incremental voltages and currents (i.e., $\mathbf{y}(s) = \Delta\mathbf{v}$, $\mathbf{u}(s) = \Delta\mathbf{i}$), the expression in (3) defines the system impedance matrix $\mathbf{Z}(s)$ [25]. This matrix contains all the dynamics of the linearized system from (2), including those of the control and the electrical components (e.g., passive filters, transmission lines, etc.). The dual expression of the impedance matrix is called the admittance matrix and can be both expressed as

$$\begin{aligned} \Delta\mathbf{u} &= \mathbf{Z}(s)\Delta\mathbf{i} \\ \Delta\mathbf{i} &= \mathbf{Y}(s)\Delta\mathbf{u} \end{aligned} \quad (4)$$

where $\mathbf{Y}(s) = \mathbf{Z}(s)^{-1}$ is the admittance matrix and $\Delta\mathbf{u} = [u_q \ u_d]^\top$, $\Delta\mathbf{i} = [i_q \ i_d]^\top$ (\top being the transpose operator) are the incremental inputs/outputs (voltages/currents) of a system in a rotating qd reference frame. From (4), it can be observed that when the elements of $\mathbf{Z}(s)$ have small values (elements of $\mathbf{Y}(s)$ have high values), a change in the current causes a small change in the voltage.

This dynamic behavior resembles the behavior of an ideal voltage source, for which the voltage remains constant independently of the current it provides. Hence, when (4) models generators, it can be considered that a generator with low element values of $\mathbf{Z}(s)$ (high element values of $\mathbf{Y}(s)$) exhibits higher voltage behavior than a source with high element values of $\mathbf{Z}(s)$ (low element values of $\mathbf{Y}(s)$). In the remaining of this section, impedance analysis will be used to analytically derive the dynamic characteristics of voltage sources behind an impedance.

B. Essential Analysis of VSBI Behaviour

The differential equations that describe the current $i_{q,d}$ flowing through a resistor R connected in series with an inductor L in a qd reference frame can be written as

$$\begin{aligned} u_q^{POC}(t) &= i_q(t)R + L\frac{di_q(t)}{dt} + \omega_0 L i_d(t) \\ u_d^{POC}(t) &= i_d(t)R + L\frac{di_d(t)}{dt} - \omega_0 L i_q(t) \end{aligned} \quad (5)$$

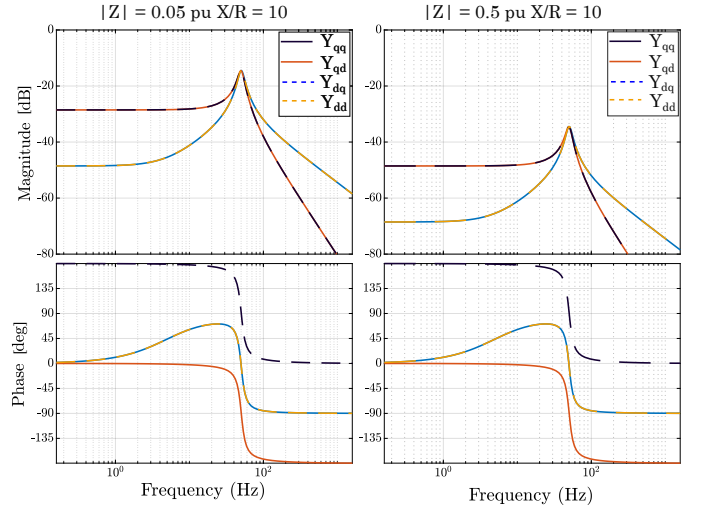


Fig. 2. Bode diagrams of the admittance matrix of the system under study with $|Z| = 0.05$ pu (left) and $|Z| = 0.5$ pu (right) with X/R ratio of 10.

where $u_{q,d}^{POC}$ are the voltage components at the Point of Connection (POC) and $\omega_0 = 2\pi f_0$ is the nominal frequency of the network. By using (2), where time dependency is removed for simplicity, (5) is rewritten as follows

$$\begin{aligned} \frac{d}{dt} \begin{bmatrix} \Delta i_q \\ \Delta i_d \end{bmatrix} &= \underbrace{\begin{bmatrix} -\frac{R}{L} & -\omega_0 \\ \omega_0 & -\frac{R}{L} \end{bmatrix}}_{\mathbf{A}} \underbrace{\begin{bmatrix} \Delta i_q \\ \Delta i_d \end{bmatrix}}_{\mathbf{x}} + \underbrace{\begin{bmatrix} -\frac{1}{L} & 0 \\ 0 & -\frac{1}{L} \end{bmatrix}}_{\mathbf{B}} \underbrace{\begin{bmatrix} \Delta u_q^{POC} \\ \Delta u_d^{POC} \end{bmatrix}}_{\mathbf{u}} \\ \begin{bmatrix} \Delta i_q \\ \Delta i_d \end{bmatrix} &= \underbrace{\begin{bmatrix} 1 & 0 \\ 0 & 1 \end{bmatrix}}_{\mathbf{C}} \begin{bmatrix} \Delta i_q \\ \Delta i_d \end{bmatrix} + \underbrace{\begin{bmatrix} 0 & 0 \\ 0 & 0 \end{bmatrix}}_{\mathbf{D}} \begin{bmatrix} \Delta u_q^{POC} \\ \Delta u_d^{POC} \end{bmatrix} \end{aligned} \quad (6)$$

By substituting matrices \mathbf{A} , \mathbf{B} , \mathbf{C} , and \mathbf{D} from (6) into (3), the admittance expression is written as

$$\begin{bmatrix} \Delta i_q \\ \Delta i_d \end{bmatrix} = \frac{1}{s^2 + \frac{2sR}{L} + \frac{R^2 + \omega_0^2 L^2}{L^2}} \begin{bmatrix} s + \frac{R}{L} & \omega_0 \\ -\omega_0 & s + \frac{R}{L} \end{bmatrix} \begin{bmatrix} \Delta u_q^{POC} \\ \Delta u_d^{POC} \end{bmatrix}. \quad (7)$$

It can be seen from (7) that second-order TFs obtained, despite the admittance having a first-order TF in each separate axis of the qd formulation. Equation (7), which is expressed in RL parameters, defines the dynamics of an ideal voltage source behind an impedance in the Laplace domain. A mapping from RL parameters to the equivalent damping and reactance-to-resistance ratios (ξ and X/R , respectively) is provided in the Appendix. Such analytical mapping provides insight into selecting the damping ratio of the user-defined reference. In the following Sections, a metric called DSI is proposed to quantify how closely potential converter control structures (both GFL and GFM) resemble the dynamic behavior defined in (7) across different frequency ranges.

To further illustrate the effect of the impedance parameter values on the dynamic behaviour of a VSBI, an example system is used, shown in Fig. 1 consisting of two Thévenin circuits. For the purpose of this analysis, two cases are considered. First, a small value for the impedance $|Z|$ is chosen equal to 0.05 pu while for the second case, its value

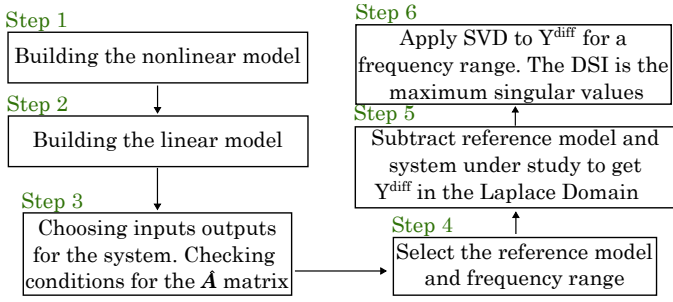


Fig. 3. Flowchart of the methodology

is increased to 0.5 pu. For both cases, an X/R ratio of 10 is chosen for Z .

Fig. 2 shows the Bode diagram of the admittance matrix of impedance Z . When $|Z|$ is set to 0.05 pu, a higher peak resonance can be observed compared to the value of 0.5 pu. This can be interpreted as presenting higher voltage source behavior. Also, since ω_0 is chosen to be 314.15 rad/s, the current will have a peak resonance in 50 Hz due to the peak observed in the Bode diagram. From the above analysis, it can be concluded that the selection of the impedance affects the VSB of the reference. By using the derived analytical expressions, and damping to X/R ratio (see Appendix) the user can customize its reference selection which will be used in DSI calculation.

III. DYNAMIC SIMILARITY INDEX

A. Proposed Method

In this section, the DSI is proposed to quantify the resemblance of a given dynamic system to a VSBI. An overview of the proposed approach can be seen in Fig. 3. First, the nonlinear model of the system is defined, as in (1). The analytical modelling of the different power system elements in the form of (1) can be found in the literature [26, 27]. Then, the nonlinear model is linearized around one operation point, resulting in the linear model of the system, as in (2). Note that, to ensure the integrity of the work, the methodology for calculating the DSI is explained starting from the development of both nonlinear and linear models. However, the methodology itself is flexible and can be applied to any linear model, regardless of how it was derived.

After obtaining the linear model, the system is separated based on the input and output selection [25]. This results in two subsystems, one representing the dynamics of the system under study (whose state matrix is \hat{A}) and the other representing the dynamics of the rest of the network, as shown in Fig. 4. For the generator, u_{qd}^{POC} is chosen as an input and i_{qd}^{tr} as an output. With this input-output selection, the admittance matrix, representing the generator and filter dynamics, is derived by transforming the equations from the state-space form of (2) to the admittance form of (4), by means of (3). Expanding upon (4), the 2×2 admittance matrix is

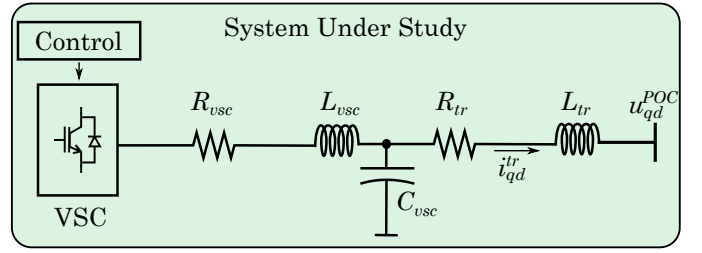


Fig. 4. System under study by choosing u_{qd}^{POC} (as input) and i_{qd}^{tr} (as output) as an example

written as follows

$$\begin{bmatrix} \Delta i_q^{tr} \\ \Delta i_d^{tr} \end{bmatrix} = \underbrace{\begin{bmatrix} Y_{qq}(s) & Y_{qd}(s) \\ Y_{dq}(s) & Y_{dd}(s) \end{bmatrix}}_{\mathbf{Y}^{sus}(s)} \begin{bmatrix} \Delta u_q^{POC} \\ \Delta u_d^{POC} \end{bmatrix} \quad (8)$$

where $u_{q,d}^{POC}$ are the qd components of the voltage at the POC and $i_{q,d}^{tr}$ are the qd components of the current flowing through the interconnection transformer. Each component of the $\mathbf{Y}^{sus}(s)$ is a TF, whose order depends on the filter topology and the complexity of the control.

In order to ensure the validity of the proposed approach, some conditions regarding the eigenvalues of matrix \hat{A} of the system under study need to be ensured. These are the following:

- 1) Matrix \hat{A} has no repeated eigenvalues.
- 2) Matrix \hat{A} has no eigenvalues with zero real part.
- 3) Matrix \hat{A} has no eigenvalues with positive real part.

Conditions 1 and 2 ensure the dynamics of the system are continuous while condition 3 ensures that the system is stable [28]. One should note that connecting two individually unstable systems can stabilize them and, conversely, separating a stable system to distinct subsystems can render the individual systems unstable [25]. For this reason, it is relevant to check the eigenvalues of the system under study state matrix \hat{A} , not the ones of the complete state matrix A .

By selecting the desired reference model, detailed in Section II, and the frequency range of interest, the methodology is applied as follows. First, the reference model is subtracted from the system under study in the Laplace domain to derive the Y^{diff} model. Note that depending on the dynamics under study, the various Y^{diff} models can be obtained. Such subtraction contains all the dynamic differences between the two models. Finally, the singular value decomposition (SVD) of the Y^{diff} model is applied over the specified frequency range, where the DSI is defined as the maximum singular value. In the subsequent subsections, the various applications of the methodology will be explained.

B. Component Level Application

In this section, the application of the DSI for the component level is discussed. Once the conditions that are explained above are met, the process to calculate the proposed DSI is the following. First, matrix $\mathbf{Y}^{sus}(s)$ is obtained by selecting the corresponding inputs and outputs in the Laplace domain (see (8)).

The same process is performed for the reference transfer function $\mathbf{Y}^{ref}(s)$, which represents the desired VSbI and is defined in (7). This results in two dynamic systems, one representing the dynamics of the system under study and one representing the desired VSbI dynamic characteristics. In order to calculate the dynamic difference between the two systems, the matrices are subtracted and an error matrix \mathbf{Y}^{diff} is achieved in the Laplace domain as follows

$$\mathbf{Y}^{diff}(s) = \mathbf{Y}^{ref}(s) - \mathbf{Y}^{sus}(s) \quad (9)$$

By applying Singular Value Decomposition (SVD) [29] to \mathbf{Y}^{diff} , the maximum (σ_{max}) singular values are calculated. Finally, the DSI is defined as

$$DSI(\omega) = \sigma_{max}(\mathbf{Y}^{diff}(\omega)) \quad (10)$$

where ω is a vector that contains the frequency points of interest. Based on its definition, the DSI represents the maximum amplification of the difference between two systems. Smaller DSIs indicate more dynamically similar systems, as the difference is not significantly amplified. On the other hand, larger DSIs demonstrate higher difference, implying that the systems are less dynamically close. It should be noted that the selection of the frequency range does not affect the accuracy of the DSI, provided that the conditions of Section III-A are met and that the linear model accurately represents the full dynamics of the system. Finally, one should note that the matrix reference \mathbf{Y}^{ref} is arbitrary and can be a user-defined dynamic system. For the purposes of this paper, the reference is a VSbI, as defined in (7), but various dynamic models can be selected depending on the application of interest.

C. System Level Application

In this section, the adaptation of the DSI to perform system-wide studies is presented. By selecting a VSbI with either a relatively high or low SCR*, (where "*" stands for the reference), the DSI can be calculated for each bus of a power system and for a range of frequency. Higher DSI values indicate lower dynamic similarity between the system under study and the selected reference, as the σ_{max} of the error matrix \mathbf{Y}^{diff} increases. When using a high SCR*, representing a strong grid, a large DSI value suggests that the bus is dynamically far from the reference, implying low or very high voltage stiffness at that bus. Conversely, when a low SCR* is used, indicative of a weak grid, large DSI values imply high or very low voltage stiffness for the bus.

Fig. 5 illustrates the methodology to properly define the impedance matrix from the point of view of each bus. In order to achieve the formulation of (4) for each point in the network, a fictitious current source is added to each bus. This current source injects virtual current in a qd reference frame with the voltages in the qd reference frame being measured at each bus of the network. With this method, a 2×2 impedance matrix consisting of TFs that contains all the network elements and control dynamics, as seen from each specific bus, is obtained for each bus. Then, by selecting a desired reference (e.g., a VSbI with a given SCR), the DSI can be calculated for a range of frequencies. Mathematically, the above can be expressed as

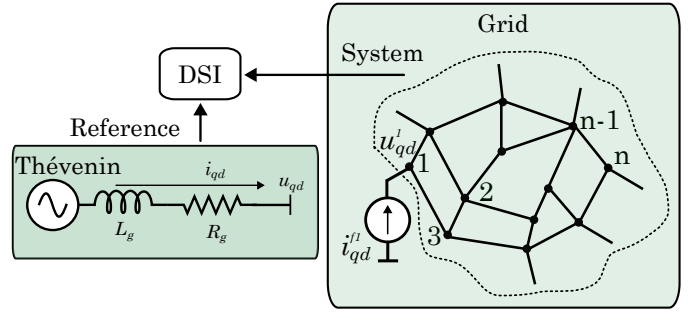


Fig. 5. Fictitious current source addition to each bus and comparison of the system with the reference by using DSI

$$\begin{bmatrix} \Delta u_q^b \\ \Delta u_d^b \end{bmatrix} = \underbrace{\begin{bmatrix} Z_{qq}^b(s) & Z_{qd}^b(s) \\ Z_{dq}^b(s) & Z_{dd}^b(s) \end{bmatrix}}_{\mathbf{Z}^{sys,b}(s)} \begin{bmatrix} \Delta i_q^{fb} \\ \Delta i_d^{fb} \end{bmatrix} \quad (11)$$

where $b \in n$ is the number of buses and f stands for fictitious. $\mathbf{Z}^{sys,b}(s)$ is the 2×2 impedance matrix in the Laplace domain. The transfer function of the reference model ($\mathbf{Z}^{ref}(s)$) can also be written in a similar way which represents the desired dynamic characteristics. Later, by subtracting $\mathbf{Z}^{ref}(s)$ and $\mathbf{Z}^{sys,b}(s)$ in the Laplace domain the $\mathbf{Z}^{diff}(s)$ can be written as follows

$$\mathbf{Z}^{diff,b}(s) = \mathbf{Z}^{ref}(s) - \mathbf{Z}^{sys,b}(s) \quad (12)$$

Hence the DSI^b , that is the DSI calculated for bus b can be written as follows,

$$DSI^b(\omega) = \sigma_{max}(\mathbf{Z}^{diff,b}(\omega)) \quad (13)$$

where $\mathbf{Z}^{diff,b}$ is the impedance error matrix calculated for each bus b . Finally, the DSI values calculated for each bus and frequency point can be written in a matrix form as follows

$$DSI^b(\omega) = \begin{bmatrix} DSI^1(1) & DSI^2(1) & \cdots & DSI^b(1) \\ DSI^1(2) & DSI^2(2) & \cdots & DSI^b(2) \\ \vdots & \vdots & \ddots & \vdots \\ DSI^1(\omega) & DSI^2(\omega) & \cdots & DSI^b(\omega) \end{bmatrix}_{[\omega \times b]}$$

IV. APPLICATION CASES OF DSI

In this section, different applications of the DSI are demonstrated. Section IV-A describes the control systems that are used in the remainder of the paper for the GFM and GFL control configurations. In Section IV-B, the DSI is applied for the VSB evaluation of converters with different control topologies and parameter settings in a radial system comprised of a single converter. In Sections IV-C and IV-D, the proposed methodology is utilized for identifying the buses with low VSB at the system level.

For the scope of this paper, the frequency ranges of study are selected as follows:

- Range 1: 0-20 Hz - Slow interaction
- Range 2: 20-40 Hz - Low frequency
- Range 3: 40-100 Hz - Converter-driven
- Range 4: 100-1000 Hz - Fast interaction

TABLE I
CASE STUDY PARAMETERS

Parameters	GFM	GFL
S_{base}	100 MVA	100 MVA
V_{base}	230 kV	230 kV
X_{vsc}	0.15 pu	0.15 pu
R_{vsc}	0.005 pu	0.005 pu
C_{vsc}	0.15 pu	0.04 pu
R_{tr}	0.002 pu	0.002 pu
X_{tr}	0.1 pu	0.1 pu
τ_{PLL}	-	0.1 s
τ_{CC}	0.001 s	0.001 s
τ_{VC}	0.01 s	-
τ_{PQ}	-	0.2 s
m_q	0.02 (pu/pu)	50 (pu/pu)
m_p	0.05 (pu/pu)	20 (pu/pu)
ω_p, ω_q	50, 10	-, -
ω_f, ω_u	-, -	50, 50

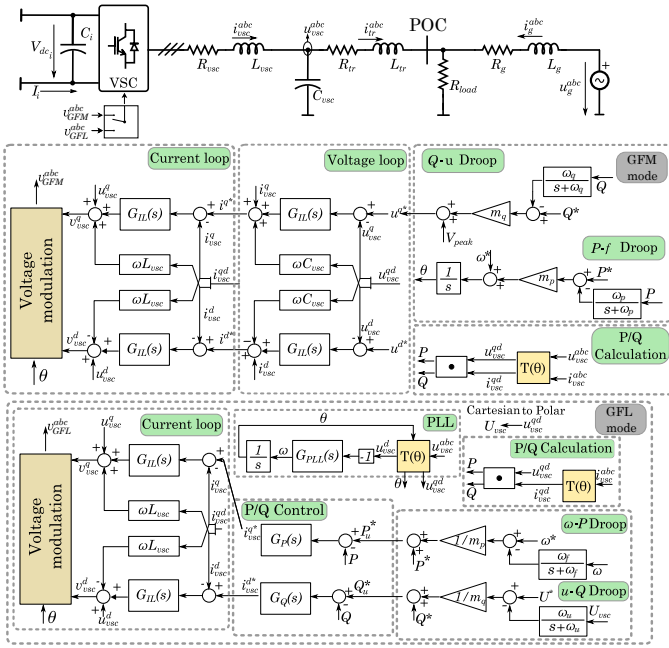


Fig. 6. GFL and GFM control topologies connected to a Thévenin grid via LCL filter topology

This range selection was chosen due to the current understanding and classification between dynamic phenomena in power systems and their timescale separation [30]. Note that different DSI can be computed for different frequency ranges, resulting in different assessments for the VSB characteristics of the bus in each frequency range.

A. Converter Control Topologies: GFM and GFL

This section presents the GFM and GFL control topologies considered in this work. It should be noted that the methodology for the VSB assessment presented in this paper is not limited to these control topologies, but can be applied to any control configuration. The presented topologies are used as representative cases of the two converter control categories. Both topologies are implemented in a qd -reference frame and in a per unit base system.

Fig. 6 shows the GFL and GFM control modes for a converter interfaced with the grid via an LC filter and a connection transformer. For both configurations, an ideal DC voltage source is assumed on the DC side. GFL converters use a PLL to synchronize with the network and to provide the angle for internal Park transformations. GFL control is also equipped with $f - P$ and $u - Q$ droops for frequency and voltage support, respectively. The droop controllers consist of a low-pass filter with cutoff frequencies ω_f and ω_u . Droop gains of m_p and m_q are used for $f - P$ and $u - Q$ droops, respectively. These droop controllers provide the active and reactive power references that are used as input signals for the cascaded power and current controllers. Both inner loops use PI controllers that are denoted with G in Fig. 6.

For the GFM converters, a $P - f$ droop is used to synchronize with the grid and to provide the converter angle for the

internal Park transformations. m_p is the droop coefficient and ω_p is the cutoff frequency of the first-order filter. The $Q - u$ droop consists of a low-pass filter with a cutoff frequency ω_q and droop coefficient m_q and provides the voltage references to the inner cascaded voltage and current controllers. The interconnection transformer is modeled as a series inductor L_{tr} and resistor R_{tr} . X_{vsc} , R_{vsc} , and C_{vsc} are the reactance, resistance, and capacitance of the converter filter respectively. Finally, R_g and L_g are the grid resistance and inductance, respectively.

B. Component Analysis: Control Performance Effect on the VSB

The objective of this subsection is to illustrate that by using the DSI, the VSB behaviour can be observed and evaluated for various tuning options of the generating units. For the study, VSB is selected as a reference with a SCR^* of 15 and X/R ratio of 10. First, the GFL and GFM modes with various control tunings are compared with a VSB to assess their VSB. Later, the time domain responses will be shown using simulation to reflect how the DSI calculations in the frequency domain translate to the time domain. Table I shows the parameters of the case study. Parameters τ_{PLL} , τ_{CC} , and τ_{VC} denote the bandwidth of the PLL, current control, and voltage control loops respectively.

For the GFL case, the closed loop time response of the outer PQ control loops τ_{PQ} is changed from 0.2 s to 0.4 s. For the GFM, the cutoff frequency (ω_p) of the $P - f$ droop is decreased from 50 to 10 while all the rest of the parameters are kept constant.

Fig. 7 shows the effect of the different parameter selection on the DSI plot for both controllers. Since the reference selected as an SCR^* of 15 and X/R 10 (which corresponds to strong VSB), it can be seen that GFM has more similarity to the selected reference than GFL. This is because the GFM controller exhibits lower DSI, so smaller error with regards to the strong VSB of the reference, compared to the GFL

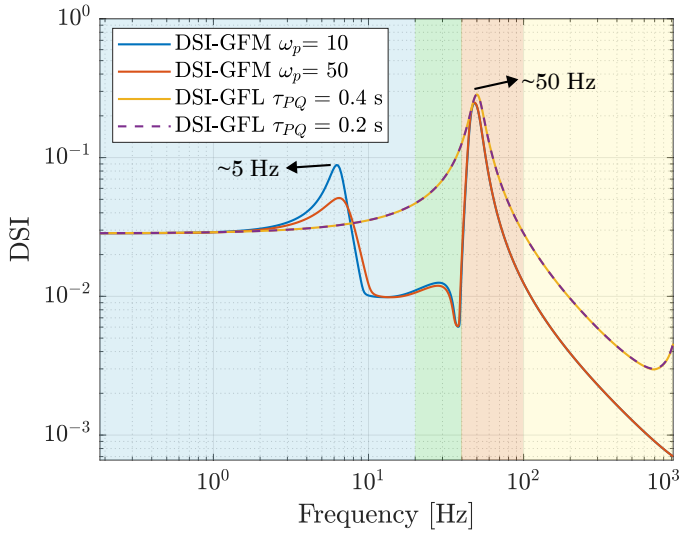


Fig. 7. Comparison of different tunings of GFL and GFM with DSI plot

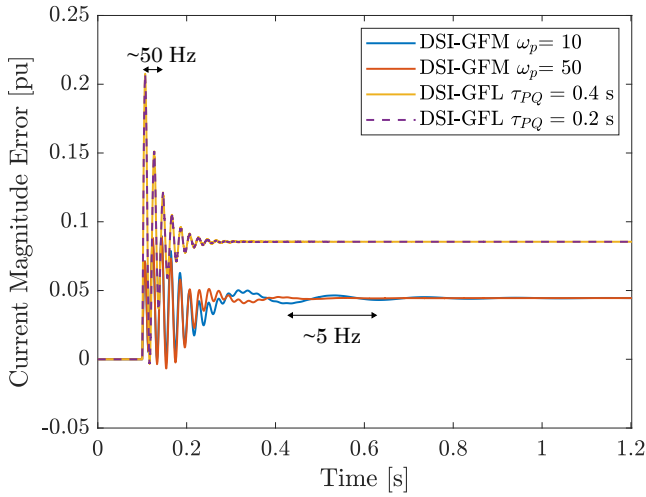


Fig. 8. Voltage step of 1% of the peak voltage at the POC. Current magnitude errors of different tuning of GFM and GFL.

one. The selection of the ω_p parameter has a significant effect around 5 Hz. This indicates an error increase in the specific frequency area. Changing the τ_{PQ} of GFL has negligible effect on the dynamics. Around the operation area of 50 Hz, the GFL controller exhibits higher DSI and thus, higher error with respect to the reference, compared to the GFM controller. Therefore, it can be concluded that the GFM controller is more similar dynamically than the GFL one to a strong voltage source across the majority of the inspected frequency range. This is consistent with the current understanding of the two different converter operation modes. The DSI provides the additional benefit of quantifying the error for the different controllers.

Fig. 8 represents the current magnitude errors with respect to the reference after a 1% POC voltage perturbation. It can be observed that GFL exhibits a higher error than GFM. For GFM with ω_p set to 10, a 5 Hz oscillation is noticeable, and the error is smaller compared to GFM with ω_p at 50. The steady-state error of GFL is higher than GFM. It can be seen

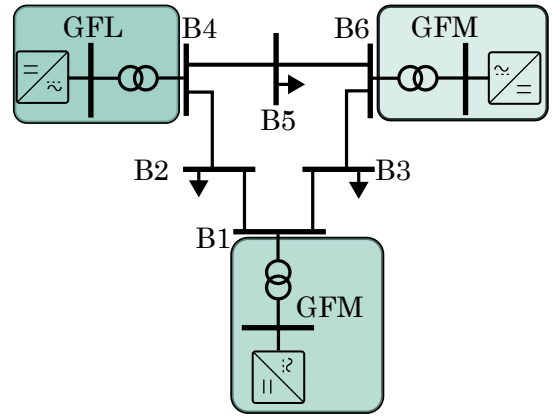


Fig. 9. Modified IEEE 9 Bus system with the addition of GFL and GFM

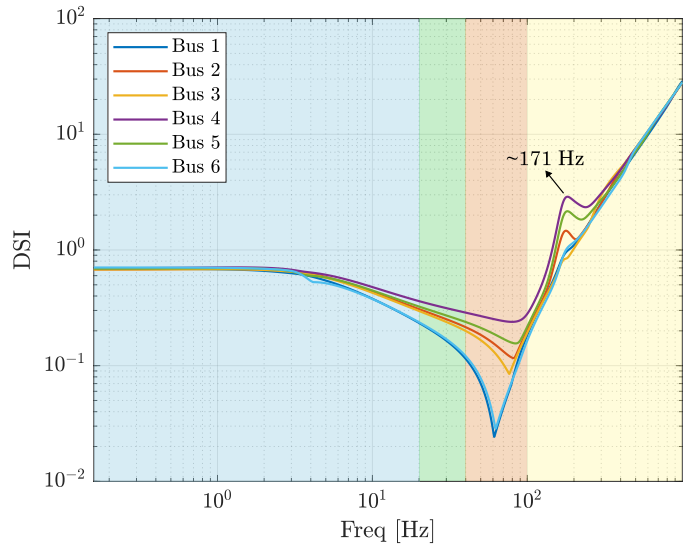


Fig. 10. DSI plot of modified IEEE 9 Bus system DSI calculated per bus

that the time domain simulation results are in good agreement with the previous DSI analysis.

C. Grid Analysis: Application for IEEE 9 Bus System

The objective of this subsection is to depict that when DSI is applied at the system level, the buses that exhibit low VSBI behaviour can be identified. The application of the DSI to the system level is demonstrated with a modified version of the benchmark IEEE 9 bus system, depicted in Fig. 9. Each bus is denoted with the letter B and, the system has a base apparent power of 100 MVA and a base voltage of 230 kV. A 310 MVA-rated GFM converter is connected to the slack bus B1. One GFL and one GFM converters are the other generation units connected to B4 and B6 with a nominal power of 280 and 260 MVA, respectively. For the dynamic reference, a VSBI with a SCR^* of 15 with an X/R ratio of 10 is selected, representing a relatively strong grid. However, depending on another study of interest another reference can be selected.

Fig. 10 represents the DSI calculated for each bus, by using the methodology presented in Section III-C. In Range 1, the DSI values are similar between the different system buses. In

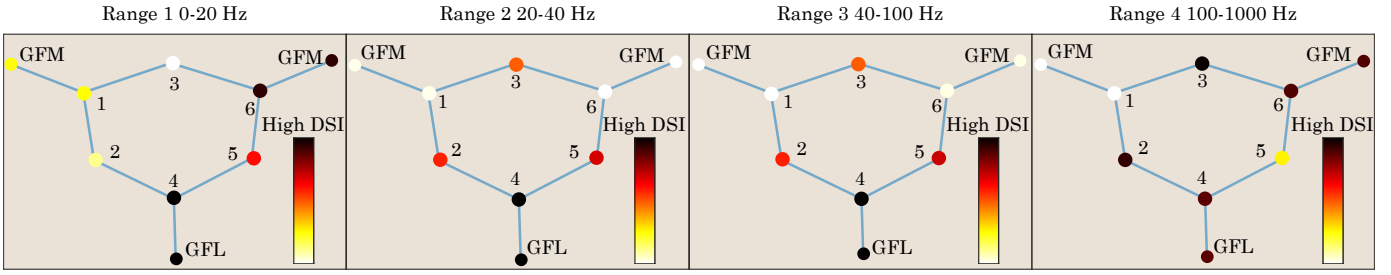


Fig. 11. Modified IEEE 9 Bus system with identified buses that have high DSI calculated per bus and represented for each range.

Ranges 2 and 3, significant variation can be observed, as buses 1 and 6 have a lower DSI than the rest of the buses and bus 4 has the highest.

This is consistent with the system topology as buses 1 and 6 have GFM converters connected to them, which demonstrate higher similarity to the selected reference in these frequency ranges. Accordingly, in such ranges GFL indicate higher dynamic error, which is consistent with the analysis and results of Section IV-A. Also, a peak in the DSI can be observed in bus 4 and 5 around 171 Hz indicating lower dynamic similarity at such frequency. Finally, at higher frequencies, the system DSI is increasing, hence reflecting an overall trend of reduced dynamic similarity to the reference.

Fig. 11 displays the modified IEEE 9 bus system as a graph for each frequency range, with a color code identifying the different values of DSI that are used in the graph. Note that for the graph presentation, the DSI values in each range are normalized based on the maximum and minimum DSI within that range. This normalization is applied solely for observation purposes, allowing independent evaluation of each frequency range.

In Range 1, bus 4 exhibits the highest DSI value, followed by buses 6 and 5, indicating that their voltage dynamics show the least similarity to the selected reference. Conversely, buses 1, 2, and 3 display lower values, suggesting a higher degree of dynamic similarity to the reference. For Range 2, bus 4 showcases the highest DSI value, indicating the lowest similarity, followed by buses 2 and 5. In Range 3, bus 1 presents the lowest value, suggesting the highest similarity to the reference, followed by buses 6 and 3. Finally, for Range 4, bus 1 has the lowest value, signifying the closest match to the reference, while the remaining buses have higher values. The above results provide insight about the voltage stiffness in the different buses of the network, based on the topology of the system and the dynamic operation of the interconnected devices, which can be leveraged for the isolation of problematic buses and guide corrective actions. Fig. 12 represents the voltage magnitude errors of buses 1, 4 and 6 with 1% of load change in load 5. For the error calculation, a reference system was used for which the converter-based generators were individually replaced by Thévenin circuit with the same impedance characteristics that were used for the DSI reference calculation. In Fig. 12 when the load at bus 5 is incremented by 1%, GFL exhibits the largest error. Notably, the voltage error of bus 1, which has GFM, is more damped than bus 4. Oscillation around 171 Hz can be observed especially in the

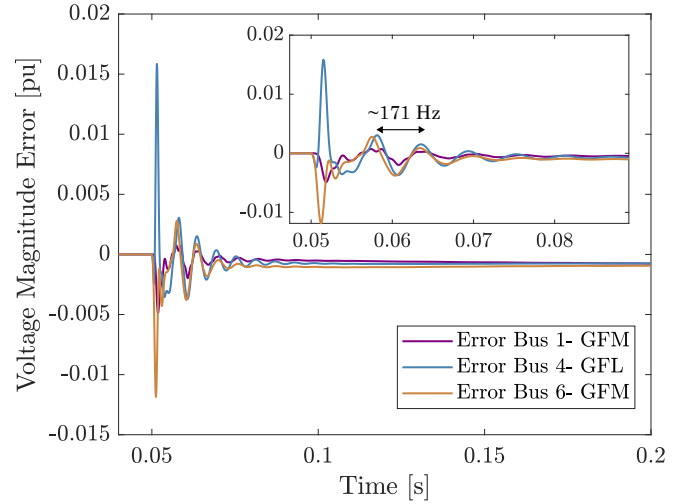


Fig. 12. Voltage magnitude errors of generation buses (1, 4, and 6) with 1% load disturbance of bus 5 including magnifying graph.

error of bus 4 which is reflected in Fig. 10 with an increment of DSI. Finally, the time domain simulation results are matching with the DSI analysis shown in Fig. 10.

D. Grid Analysis: Application for IEEE 118 Bus System

The objective of the subsection is to show the scalability of the proposed method and the calculation efficiency of the system-wide DSI, the same analysis was applied to a modified version of the well-known IEEE 118 bus system. The system under study is shown in Fig. 13, with 12 generation units operating in GFL mode (in blue), and 16 operating in GFM mode (in green). The total GFL penetration is 28.6 % with respect to the total nominal power. For the DSI reference, the same impedance parameters were used as in the previous cases while similar normalization was used as in the 9 bus case. The number of states was increased to 1159 states from 73, compared to the 9 bus case.

Fig. 14 presents the system as a graph with the DSI values for each bus and for the different frequency regions of the study. For Range 1, buses 112, 110, and 117 display higher DSI values indicating a dynamically distant behavior compared to the selected reference for the rest of the buses. However, buses such as 31, 32, 27, and 29 have low DSI values which show the most dynamic similarity compared to the selected reference. For Range 2 and 3, bus 86 has the highest DSI followed by 72 and 117, implying the biggest

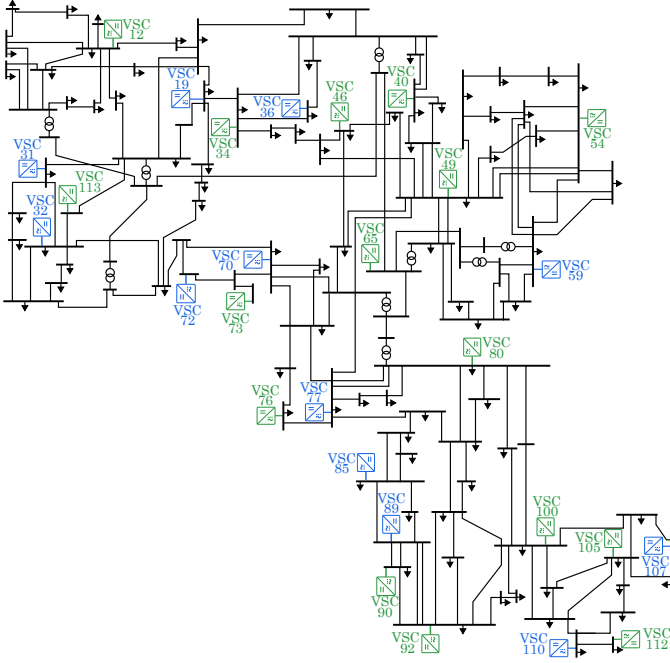


Fig. 13. Modified IEEE 118 Bus system including 12 GFL (blue) and 16 GFM (green)

TABLE II
COMPUTATION TIME OF THE IEEE 9 AND 118 BUS SYSTEMS

	9 Bus (73 states)	118 Bus (1159 states)
State-space calculation	7 s	9 s
Condition checking	0.2 s	39.3 s
DSI calculation	0.5 s	3616 s
Total	7.7 s	3664.3 s

error for the selected reference and, the rest of the buses have low DSI values. Finally, for Range 4, bus 42 has the highest DSI, however, buses such as 13, 14 and 16 have low DSI values showing more similarity to the selected reference than the rest of the buses. So, considering the above results, the modified IEEE 118 Bus system with such topology and selected reference, buses 42, 72, 86, and 117 has the lowest similarity to a VSbI with a SCR* of 15 and X/R of 10, indicating that such buses are more susceptible to voltage variations from the rest of the buses. The results from the above analysis can be used for the identification of problematic parts of the network and for resiliency enhancing, system-level planning.

Table II shows the necessary computation time for applying the proposed method for the 9 and 118 bus cases, divided between each necessary step (see Fig. 3). The state-space calculation is done automatically in Matlab taking into account the topology of each system, hence no notable difference is observed for the two systems. The necessary time to perform the condition checking, detailed in Section III, of 118 bus system is 196 times higher than the 9 bus case. For the 9 bus DSI calculation, 0.5 seconds were required to calculate the DSI while for the 118 bus system, 3616 seconds (~ 60.21 minutes)

were required. One should note that computation time can vary significantly depending on the control design complexity, network size, and frequency resolution which, for this study, was set to a step of 0.15 Hz for a range of 0-1000 Hz. The calculations were performed on a 13th Gen Intel(R) Core(TM) i7-1355U 1.70 GHz processor with 40 GB RAM.

V. CONCLUSION

This paper proposes a dynamic similarity index that quantifies the difference dynamic responses of two systems. This index is calculated for a range of frequencies by including all the desired dynamics. In order to apply the DSI, a reference model is selected for the comparison against a desired dynamic response. In this work, a VSbI is selected as a reference and two applications of the DSI are performed by using such reference. It is shown that, applying DSI to a single component evaluates its dynamic performance against a desired reference, reflecting, in this particular case, the VSB of the converter control. At the system level, DSI diagnoses buses with low VSB, providing critical insights into grid strength, currently defined as SCR. Future work will focus on defining alternative references to present VSB or other dynamic responses, beyond the conventional VSbI for the DSI calculation, as well as on optimizing the control setup of a converter to minimize its dynamic error from a desired reference.

APPENDIX A

ANALYTICAL DERIVATION OF DAMPING RATIO

The analytical relationship between impedance parameters R and L and design specifications X/R and ξ (damping ratio) is derived in this Appendix.

Starting from the second order TF of equation (7) and by setting $k = R/L$, considering the second order expression $as^2 + bs + c$, the following relations are derived

$$a = 1, b = 2k, c = k^2 + \omega^2. \quad (14)$$

The discriminant D can be computed as follows

$$D = b^2 - 4ac, \sqrt{D} = -j2\omega. \quad (15)$$

The poles can be calculated as follows

$$x_{1,2} = \frac{-b \pm \sqrt{D}}{2a} \quad (16)$$

$$= -k + j\omega. \quad (17)$$

The damping factor $\xi = \frac{k}{\sqrt{k^2 + \omega^2}}$ can be rewritten as follows

$$\xi \sqrt{(k^2 + \omega^2)} = k. \quad (18)$$

Taking the square of (18) and solving for k we derive

$$k = \frac{\xi\omega}{\sqrt{1 - \xi^2}}. \quad (19)$$

Substituting back $k = \frac{R}{L}$ into (19)

$$\frac{R}{L} = \frac{\xi\omega}{\sqrt{1 - \xi^2}}. \quad (20)$$

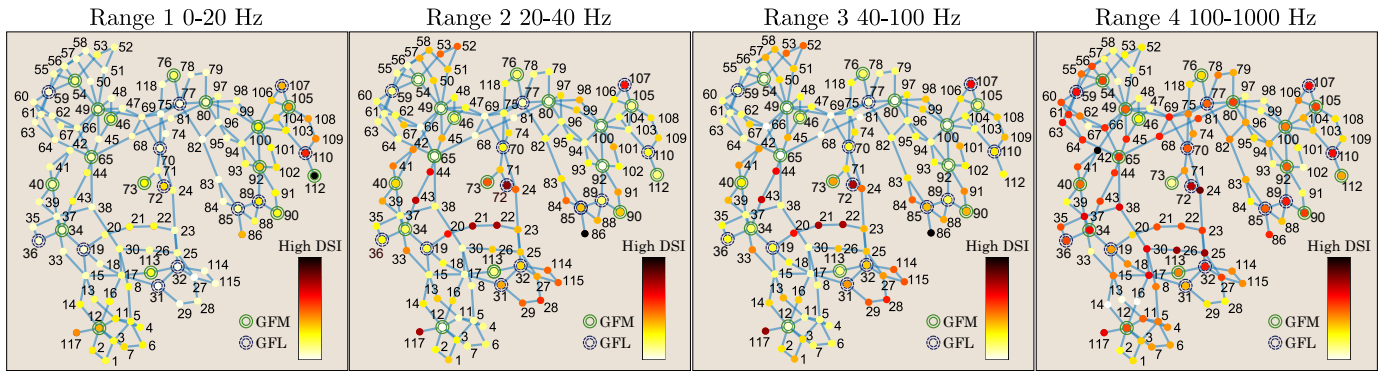


Fig. 14. Modified IEEE 118 Bus system including 12 GFL and 16 GFM converters with identified buses that have high DSI calculated per bus and represented for each range.

Replacing $L = \frac{X}{\omega}$ and isolating ξ we can write

$$\xi = \frac{R}{\sqrt{X^2 + R^2}}. \quad (21)$$

ACKNOWLEDGMENT

This work was supported by FEDER / Ministerio de Ciencia e Innovación - Agencia Estatal de Investigación, under the project REFORMING (PID2021-127788OA-I00). The work of O. Gomis was supported by the ICREA Academia program. The work of E. Prieto and M. Cheah was supported by Serra Hünter Program. The work of J. Amorós has been partially supported by the project PID2023-146936NB-I00 financed by the Spanish State Agency MCIN/AEI, FEDER, UE.

REFERENCES

- [1] P. Kundur, *Power System Stability and Control*. McGraw-Hill Companies, 01 1994.
- [2] A. A. Sallam and O. P. Malik, *Power system stability : modelling, analysis and control*. Institution Of Engineering And Technology, 2015.
- [3] ENTSO-E, “High penetration of power electronic interfaced power sources (hpopeips),” 2017.
- [4] IEA, “Global energy review,” 2021.
- [5] D. Moutevelis, J. Roldán-Pérez, M. Prodanovic, and F. Milano, “Taxonomy of power converter control schemes based on the complex frequency concept,” *IEEE Trans. on Pow. Sys.*, 2023.
- [6] M. Paolone *et al.*, “Fundamentals of power systems modelling in the presence of converter-integrated generation,” *Electric Power Systems Research*, vol. 189, p. 106811, 2020.
- [7] ENTSOE, “High penetration of power electronic interfaced power sources and the potential contribution of grid forming converters,” p. 32, 2019.
- [8] J. Matevosyan *et al.*, “A future with inverter-based resources: Finding strength from traditional weakness,” *IEEE Power and Energy Magazine*, vol. 19, no. 6, pp. 18–28, 2021.
- [9] X. Wang, M. G. Taul, H. Wu, Y. Liao, F. Blaabjerg, and L. Harnefors, “Grid-synchronization stability of converter-based resources—an overview,” *IEEE Open Journal of Industry Applications*, vol. 1, pp. 115–134, 2020.
- [10] R. Rosso, X. Wang, M. Liserre, X. Lu, and S. Engelken, “Grid-forming converters: Control approaches, grid-synchronization, and future trends—a review,” *IEEE Open Journal of Industry Applications*, vol. 2, pp. 93–109, 2021.
- [11] “Grid-forming technology in energy systems integration es energy systems integration group,” 2022, eSIG report. [Online]. Available: <https://www.esig.energy/reports-briefs>.
- [12] D. Rathnayake *et al.*, “Grid forming inverter modeling, control, and applications,” *IEEE Access*, vol. PP, pp. 1–1, 08 2021.
- [13] F. Zhao, X. Wang, and T. Zhu, “Power dynamic decoupling control of grid-forming converter in stiff grid,” *IEEE Transactions on Power Electronics*, vol. 37, pp. 9073–9088, 8 2022.
- [14] —, “Low-frequency passivity-based analysis and damping of power-synchronization controlled grid-forming inverter,” *IEEE Journal of Emerging and Selected Topics in Power Electronics*, vol. 11, pp. 1542–1554, 4 2023.
- [15] Z. Xu, N. Zhang, Z. Zhang, and Y. Huang, “The definition of power grid strength and its calculation methods for power systems with high proportion nonsynchronous-machine sources,” *Energies*, vol. 16, 2023.
- [16] S. Shah, P. Koralewicz, V. Gevorgian, and R. Wallen, “Sequence impedance measurement of utility-scale wind turbines and inverters - reference frame, frequency coupling, and mimo/siso forms,” *IEEE Transactions on Energy Conversion*, vol. 37, pp. 75–86, 3 2022.
- [17] J. M. Julia Matevosyan, “Grid-forming technology in energy systems integration es energy systems integration group,” 2022. [Online]. Available: <https://www.esig.energy/reports-briefs>.
- [18] K. Vatta Kkuni, S. Mohan, G. Yang, and W. Xu, “Comparative assessment of typical control realizations of grid forming converters based on their voltage source behaviour,” *Energy Reports*, vol. 9, pp. 6042–6062, 2023.
- [19] H. Xin, C. Liu, X. Chen, Y. Wang, E. Prieto-Araujo, and L. Huang, “How many grid-forming converters do we need? a perspective from small signal stability and power grid strength,” *IEEE Transactions on Power Systems*, pp. 1–13, 2024.
- [20] I. J. Perez-arriaga, G. C. Verghese, and F. C. Scheweppe, “Selective modal analysis with applications to electric power systems, part i: Heuristic introduction,” *IEEE Transactions on Power Apparatus and Systems*, vol. PAS-101, pp. 3117–3125, 1982.
- [21] J. Machowski, J. W. Bialek, and D. J. Bumby, *Power System Dynamics*. John Wiley & Sons, 2011.
- [22] C. A. Canizares, “Calculating optimal system parameters to maximize the distance to saddle-node bifurcations,” *IEEE Transactions on Circuits and Systems I: Fundamental Theory and Applications*, vol. 45, no. 3, pp. 225–237, 1998.
- [23] Y. Chen, R. Preece, and M. Barnes, “Improving system loadability with the consideration of multiple bifurcations,” *International Journal of Electrical Power & Energy Systems*, vol. 132, p. 107182, 2021.
- [24] K. Ogata, *Modern control engineering fifth edition*, 2010.
- [25] J. Sun, “Impedance-based stability criterion for grid-connected inverters,” *IEEE transactions on power electronics*, vol. 26, no. 11, pp. 3075–3078, 2011.
- [26] D. Moutevelis, J. Roldán-Pérez, M. Prodanovic, and S. Sanchez-Acevedo, “Bifurcation analysis of active electrical distribution networks considering load tap changers and power converter capacity limits,” *IEEE Transactions on Power Electronics*, vol. 37, no. 6, pp. 7230–7246, 2022.
- [27] C. Collados-Rodriguez, M. Cheah-Mane, E. Prieto-Araujo, and O. Gomis-Bellmunt, “Stability analysis of systems with high vsc penetration: Where is the limit?” *IEEE Transactions on Power Delivery*, vol. 35, no. 4, pp. 2021–2031, 2020.
- [28] Y. Kuznetsov, *Elements of Applied Bifurcation Theory*. Springer Science & Business Media, 2008.
- [29] S. Skogestad and I. Postlethwaite, *Multivariable Feedback Control*. John Wiley & Sons, 11 2005.
- [30] N. Hatziazygiou *et al.*, “Definition and classification of power system stability – revisited & extended,” *IEEE Transactions on Power Systems*, vol. 36, no. 4, pp. 3271–3281, 2021.